SEVENTH EUROPEAN ROTORCRAFT AND POWERED LIFT AIRCRAFT FORUM

Paper No. 76

A SIMPLE SYSTEM FOR HELICOPTER INDIVIDUAL-BLADE-CONTROL AND ITS APPLICATION TO STALL FLUTTER SUPPRESSION

Norman D. Ham

Todd R. Quackenbush

Department of Aeronautics and Astronautics
Massachusetts Institute of Technology
Cambridge, Massachusetts 02139

September 8 - 11, 1981

Garmisch-Partenkirchen
Federal Republic of Germany

Deutsche Gesellschaft für Luft- und Raumfahrt e. V.

Goethestr. 10, D-5000 Köln 51, F.R.G.

A SIMPLE SYSTEM FOR HELICOPTER INDIVIDUAL-BLADE-CONTROL AND ITS APPLICATION TO STALL FLUTTER SUPPRESSION

Norman D. Ham*

Todd R. Quackenbush**

Department of Aeronautics and Astronautics
Massachusetts Institute of Technology
Cambridge, Massachusetts 02139

Abstract

A new, advanced type of active control for helicopters and its application to a system for stall flutter suppression is described.

The system, based on previously developed M.I.T. Individual-Blade-Control hardware, employs blade-mounted accelerometers to sense torsional oscillations and feeds back rate information to increase the damping of the first torsion mode. A linear model of the blade and control system dynamics is used to give qualitative and quantitative guidance in the design process as well as to aid in analysis of experimental results. System performance in wind tunnel tests is described, and evidence is given of the system's ability to provide substantial additional damping to stall-induced blade oscillations.

1. Introduction

A truly advanced helicopter rotor must operate in a severe aerodynamic environment with high reliability and low maintenance requirements. This environment includes:

(1) atmospheric turbulence (leading to impaired flying qualities, particularly in the case of hingeless rotor helicopters).

(2) retreating blade stall flutter (leading to large torsional loads in blade structure and control system).

(3) blade-vortex interaction in transitional and nap-of-the-earth flight (leading to unacceptable higher harmonic blade bending stresses and helicopter vibration).

(4) blade-fuselage interference (leading to unacceptable higher harmonic blade bending stresses and helicopter vibration).

(5) blade instabilities due to flap-lag coupling and high advance ratio (including blade "sailing" during shut-down).

The application of feedback techniques make it possible to alleviate the effects described in items (1) to (5) above, while improving helicopter vibration and handling characteristics to meet desired standards. The concept of Individual-Blade-Control (IBC) embodies the control of broad-band electrohydraulic actuators attached to the swash plate (or individually to each blade), using signals from sensors mounted on the blades to supply appropriate control commands to the actuators[1,2]. Note that the IBC involves not just control of each blade independently, but also a feedback loop for each blade in the rotating frame. In this manner it becomes possible to reduce the severe effects of atmospheric turbulence, retreating blade stall flutter, blade-vortex interaction, blade-fuselage interference, and blade instabilities, while providing improved flying qualities.

It is evident that the IBC system will be most effective if it is comprised of several sub-systems, each controlling a specific mode, e.g., the blade flapping mode, the first blade inplane mode, the first blade flatwise bending mode, and the first blade torsion mode. Each sub-system operates in its appropriate frequency band.

The configuration used in this investigation employs an individual actuator and multiple feedback loops to control each blade. These actuators and feedback loops rotate with the blades and, therefore, a conventional swash plate is not required. However, actuator reliability considerations may outweigh the simplicity of this configuration: in practice, the same degree of individual-blade-control can be achieved by placing the actuators in the non-rotating system and controlling the blades through a conventional swash plate. The actual configuration then depends upon the number of blades:

No. of Blades	Collective	Differential Collective	Longitudinal Cyclic	Lateral Cyclic
2	X	X		
3	X		X	X
4	X	X	X	X

Note that individual-blade-control can thus be achieved in the non-rotating system if the number of control degrees-of-freedom equals the number of blades. For more than three blades, the use of extensible blade pitch control rods in the form of hydraulic actuators is a possibility.

The present paper is concerned with the application of the Individual-Blade-Control concept to blade stall flutter suppression.

In forward flight, the high blade angles of attack on the retreating side and their rapid

This research was sponsored by the Ames Research Center, NASA, Moffett Field, California 94035. Major contributions to the project were made by P.H. Bauer and R.M. McKillip, Jr.

*Director, VTOL Technology Laboratory.
**Research Engineer.

variations cause dynamic stall-induced blade torsional oscillations for certain combinations of blade torsional natural frequency, blade loading, and advance ratio; the spanwise integrated effect of dynamic stall is to feed energy into blade torsional motion[3]. This motion is generally only transiently unstable and damps out rapidly as the blade rotates toward the advancing side. However, the one or two cycles of blade motion that do occur are sufficient to put extreme loads on the rotor control system (see Fig. 1[3]); the fatigue life of blade pitch links is considerably reduced.

Applying Individual-Blade-Control (IBC) techniques to this problem offers a possible solution. Reference 2 showed that appropriate feedbacks to a position control servo governing blade pitch motion could reduce undesirable blade motions due to low-frequency gust inputs. It was felt that similar methods could be applied to alleviate the violent torsional motions associated with stall flutter. As noted previously, at high blade angles of attack and certain reduced frequencies, aerodynamic moment hysteresis causes a net input of energy to blade torsional motion, so that any small blade oscillation grows with time. Such a situation is typical of simple oscillating systems with negative damping; stall flutter can be conceived of as a phenomenon caused by a once-per-revolution variation in the effective damping of the blade in pitch. On the advancing side, the blade experiences strong positive damping at low angles of attack, but on the retreating side the effective damping can temporarily become negative, leading to the oscillations described above. Figure 2, from Ref. 3, shows the variation of the effective pitch damping with blade operating condition.

An effective stall flutter suppression system, then, would eliminate this one-per-rev excursion into negative damping. One way to achieve this end is to provide pitch-rate feedback from the blade to the pitch control servo. The details of this concept, its implementation, and the results of experiments utilizing it are given in the following sections.

2. Model Design and Description

The model used here to test the proposed stall flutter suppression system was identical in most particulars to that used in Ref. 2. A D.C. servomotor acting as a blade pitch position control system was mounted on the rotor shaft. The test rotor used only a single blade, with a NACA 0012 section, 21.2 inch span, and a two inch chord; further details of the blade are given in Table 1. The blade was attached to the rotor hub by means of a steel fork which in turn was connected to a spherical bearing; thus the blade's flapping, lagging, and feathering motions all took place about the same point. A steel flexure instrumented with strain gauges was attached to the blade to sense pitch angle.

Two "dummy blades" in the form of lengths of threaded 5/8" steel rod were also attached to the rotor hub. Each rod had adjustable counterweights which were used to achieve dynamic balancing during rotor operation. Two symmetrically mounted counterweights were also attached to the shaft to balance the active motor.

Photographs at the blade and control system hardware are shown in Figs. 3 and 4. Further details of the construction of the actuation system are given in Ref. 2 and will not be repeated here.

Since the primary aim of this experiment was to design a system to control the first torsion mode of the rotor, it was necessary to ensure that the frequency of the mode was within the bandwidth of the servomotor. For full scale rotor blades, ω_θ is usually of the order of 5Ω to 7Ω, or about 30-40 Hz for most helicopters. Since for full-scale blades, most of the torsional flexibility originates in the control system itself, such flexibility was introduced into the model blade by inserting two leaves of spring steel (dimensions 3-1/2" x 1-1/8" x .02") between the blade mounting fork and blade itself (see Fig. 4). As shown in Fig. 4, the leaves were installed so that they were parallel to the plane of the blade. This modification (which added 3.5" to the blade radius) was achieved by bolting one end of the leaves to the mounting fork which originally clamped directly onto the blade (with the aid of steel spacing plates in the fork); the other ends of the leaves were secured to the blade with the aid of two 2-1/4" x 1-1/4" x 3/16" aluminum clamping plates built for this purpose (steel spacers were again used between the clamping plates).

As noted in Section 1, the principal aim of this experiment was to increase the damping of blade torsional oscillations by supplying a pitch rate feedback to the blade control system. The pitch rate signal was obtained by integrating a pure pitch acceleration signal from accelerometers mounted on the blade. Any single accelerometer mounted away from the pitching axis will sense a component of centrifugal force (the origin of the so-called "propeller moment") which is proportional to pitch angle. This difficulty can be overcome if the signals from two separate accelerometers mounted of an equal distance from the pitching axis but oriented with a 90° separation between them are summed; the result is a signal purely proportional to $\ddot{\theta}$, as shown below.

In the simplest case shown in Fig. 5, for a blade pitching up at instantaneous pitch angle θ, an accelerometer at a point ℓ from the blade pitching axis and in the plane of the blade senses an inertia force proportional to

$$a_1 = \ell\ddot{\theta} + \ell\Omega^2 \sin\theta \cos\theta$$

while an accelerometer at a distance ℓ from the blade pitching axis and perpendicular to the plane of the blade senses

$$a_2 = \ell\ddot{\theta} - \ell\Omega^2 \sin\theta \cos\theta$$

If the above inertia forces are sensed by two accelerometers and the signals summed, the result is

$$a_1 + a_2 = 2\ell\ddot{\theta}$$

The above result is strictly true only if the flapping and lagging degrees of freedom are neglected. Unless the accelerometers are placed such that they lie in the plane formed by the lagging and flapping axes, components of centrifugal force proportional to lag angle ζ and flap angle β will enter into the signal sensed by the accelerometers. This situation has the potential for causing difficulties with the integrated feedback signal, since an ideal integrator would apply an infinite D.C. gain to any steady-state components in the ζ and β signals. However, the integrator used had a roll-off at low frequencies (below approximately 0.5 Hz) which eliminated all steady-state signals.

The accelerometer installation described above will sense a strong 1Ω signal due to cyclic pitch input. This circumstance will not interfere with the intended purpose of this feedback control system (i.e., providing additional damping to transient disturbances in torsion) since the 1Ω is a steady input; a rate feedback on such a signal will merely introduce a phase lag which can be compensated for elsewhere in the pitch control system.

Further details of the complete system are given in Ref. 4.

3. Theoretical Considerations

The system equations of motion and the overall system dynamics are derived in detail in Ref. 4.*

The block diagram of the system is shown in Fig. 6 and the root locus diagram is shown in Fig. 7 for $K_\theta = .528$ and $K_{\dot{\theta}} = .19$. These values of K_θ and $K_{\dot{\theta}}$ were chosen since they gave what appeared to be an acceptably large range of values in which the rate feedback could stabilize the blade oscillations.

Note that the system dynamics detailed above neglect the effects of aerodynamic damping (be it positive or negative) on the blade. Inserting a term $D_A\dot{\theta}$ in the equations of motion to account crudely for aerodynamic damping shows that the *effect of aerodynamics is to move the blade* oscillation pole of Fig. 7 to the right with negative D_A, while oscillation frequency is nearly constant; for sufficiently large, negative values of D_A the pole is driven into the right half-plane, but only transiently, since D_A and, thus, pole location vary with azimuth. For proper choices of $K_{\dot{\theta}}$ and K_p though, blade oscillations can be stable all around the azimuth (again see Fig. 7); nor should the value of K_p required to stabilize the pitch oscillations be excessive, since the effective "negative damping ratios" associated with stall-induced instabilities are rather small ($\zeta_{eff} \cong -0.1$ at a maximum).

*Also see Appendix.

Figure 7 illustrates two interesting aspects of the model presented here. First, the root locus diagram indicates that the blade oscillation frequency will increase substantially as K_p is increased. Second, the analysis predicts that the oscillation will be stabilized for only a certain range of K_p values and will develop a relatively high-frequency, potentially unstable oscillation if K_p is increased sufficiently. As will be discussed in Section 4, both qualitative and quantative agreement was found between the predictions made above and actual experimental results.

Finally, as is evident from the above discussion, detailed aerodynamic or structural analysis was not done preparatory to the experiments described herein; this circumstance came about fundamentally because such analysis was impracticable and unnecessary given the intended scope of the present work. A number of detailed and complex analyses of stall flutter and its effects or rotor blades have already been performed with powerful computational tools and elaborate models. Since the system to be designed and tested here was to be proof-of-concept, the simple dynamic and aerodynamic models used above were adequate. This evaluation was borne out by the results presented in Section 4.

4. Test Results and Discussion

Testing of the I.B.C. stall flutter suppression system was performed in the M.I.T. Wright Brothers Wind Tunnel. The 7' x 10' test section contained two vertical trunnions which supported the rotor shaft in a horizontal attitude. This orientation, which caused the rotor to rotate in a vertical plane, was a result of the mounting requirements of the previous series of I.B.C. gust alleviation tests (Ref. 2). One consequence of this orientation was to introduce a one-per-rev gravity pulse into the accelerometers used in the control system; however, the magnitude of the pulses was sufficiently small that no adverse effect on system performance was expected or observed.

The rotor was driven by an external hydraulic motor. The shaft was equipped with slip rings to provide power to the servomotor and to extract data from the various sensing elements. On-line data extraction was accomplished using software previously developed by other members of the I.B.C. project team.

A series of tests were run with the blade static, in hover, and in forward flight at two separate advance ratios. The static tests were designed to establish the fundamental workability of the proposed control system. Before these tests were conducted, a choice had to be made concerning the number of steel leaves to be inserted between the actuator and the blade, since the number of leaves determines the natural frequency of the torsional spring. One leaf yielded a torsional frequency of approximately 17 Hz, while two leaves yielded 31 Hz, and three leaves 42 Hz. The two-leaf configuration was chosen since the frequency

fell within the bandwidth of the servo and also provided sufficient flapwise stiffness to prevent interference between the blade and the shaft support trunnions during rotor run-up.

In the static tests the blade was hung vertically downward from the shaft while an external pulse train of frequency 6.7 Hz was introduced to excite blade motion. For these tests, and for all succeeding tests, three separate levels of K_p (0.0, 0.13, and 0.26) were established as benchmarks which covered the significant range of system performance. The rate and acceleration responses of the blade to the identical pulse input for K_p = 0 and 0.26 are shown in Figs. 8 and 9. Graphic representations of the Fast Fourier Transform of the pitch rate signals for K_p = 0.0 and K_p = .26 are shown in Fig. 10. Both of these sets of results reflect the trends predicted in Section 3; the damping of the blade first torsion mode is increased with increasing K_p, while the frequency of the oscillation increases. Note that the values of K_p used here correspond to the indicated points on the root locus diagram of Fig. 7. These values correspond to blade oscillations with ζ = .06 and damped natural frequency of 208 rad/sec (for K_p = .13) and ζ = .085 and damped natural frequency of 224 rad/sec (for K_p = .26). These values can be compared to values of .15 and 212 rad/sec, respectively, for K_p = .13, and .24 and 233 rad/sec, respectively for K_p = .26, that were observed experimentally. These results suggest that there was considerably more damping present in the system than that predicted by the theoretical model. This is not too surprising, since only the mechanical friction of the motor itself was included in the theoretical model; many other possible sources of friction (e.g. gear meshing, linkage friction) doubtless existed but were difficult to include in a linear model and so were neglected. The relatively close agreement of the frequency predictions, though, was encouraging, as was the fact that the model predicts that the system will go unstable at high gain at 70 Hz, which agreed reasonably closely with the 65 Hz observed in experiments.

Unfortunately, the usefulness of the theoretical model is limited to the static rotor cases. The time-varying aerodynamic damping in the hover and forward flight cases introduces sufficient additional complications that detailed predictions with this model, which neglects aerodynamic effects, become invalid. However, as will become apparent in the following discussion, the overall functioning of the system is not impaired by this circumstance.

To summarize, then, the effective damping ratio of the K_p = 0.0 case was .02, while for K_p = .13 it was .15, and for K_p = .26 it was .24. From Fig. 10, one also notes that the pitch rate component at ω_θ was decreased dramatically relative to the K_p = 0.0 case with K_p = .26. These results again show the strong potential of this system for increasing the damping of torsional oscillations in the 30-40 Hz frequency range.

The next step in testing was to run three cases with the rotor operating in hover and with external pitch excitation supplied. Ordinarily, it is possible (see Ref. 3) to induce stall flutter in hover by raising collective pitch until the blade stalls and provides the necessary excitation. However, the pitch linkage on the model rotor had not been specifically designed to operate at high collective, and the maximum settings available (16°-17°) were insufficient for the deep blade stall needed, so once again resort was made to external excitation.

For these hover tests, the rotor was operated at 15° collective. Rotor rotation frequency was 6.7 Hz, and the frequency of external excitation was usually 6.7 Hz, while the magnitude of each input pulse varied from case to case (though it was never more than approximately 2° or 0.63 volts). A comparison of the pitch rate response for K_p = 0.0 and for K_p = 0.26 showed the effective damping ratio for K_p = 0.0 to be 0.03, while for K_p = .26 it was 0.14. A comparison of the FFT breakdowns of the pitch acceleration response for the two cases again showed the large decreases in acceleration components in the vicinity of ω_θ = 31 Hz.

To complete the testing series, two sets of forward flight cases at moderate advance ratio were run. In these cases it was found that stall flutter could be brought about and, thus, resort did not have to be made to external pitch excitation. For the first set of runs, rotation frequency was 6.7 Hz, tunnel speed was 20 mph, and hence advance ratio was 0.30. Root collective pitch was 16° and a one-per-rev cyclic pitch signal of $\pm$9.0° was superimposed, with the maximum pitch angle reached at ψ = 270°. A second set of forward flight experiments was performed at essentially the same collective, cyclic, and wind speed settings, though the advance ratio was increased to 0.33 by decreasing Ω to 6.1 Hz. This flight condition induced a substantially stronger stall flutter oscillation than in the previous case, so much so that, as seen in Fig. 11, K_p could not be reduced to zero, only to .02, lest a violent oscillation develop. Even with this stronger excitation, though, settings of K_p = .13 and .26 were sufficient to damp out the torsional oscillations to a substantial degree (see Figs. 12-14). It is interesting to note that most of the beneficial effect of the feedback was obtained with K_p = .13; increasing K_p to .26 produced only a marginal further improvement: this result is similar to the predictions of Fig. 7 for the static case.

The pitch control perturbations required to produce the favorable results of Figs. 12-14 were minimal, as shown in Fig. 15. The corresponding control frequency spectra are shown in Fig. 16.

Further details of the test results are given in Ref. 4.

5. Conclusions

From the preceding calculations and experiments, the following conclusions can be drawn:

(1) Treating stall flutter as a phenomenon induced by time-varying aerodynamic damping serves as an effective point of departure for analysis and design of a stall-flutter-suppression system.

(2) A relatively simple linear model of the blade and servomotor dynamics can serve to give substantial quantitative and qualitative guidance as to feedback gain selection for a stall flutter suppression system based on I.B.C. techniques.

(3) A system centered around the concept of providing rate feedback to the blade control motor from blade-mounted accelerometers can generate substantially increased damping of first mode torsional oscillations induced by either mechanical or aerodynamic excitation.

(4) No apparent fundamental obstacle exists to extending the control techniques developed to larger scale systems.

References

1. Ham, N.D., "A Simple System for Helicopter Individual-Blade-Control Using Modal Decomposition", Vertica, 4, 1, 1980.

2. Ham, N.D. and McKillip, R.M. Jr., "A Simple System for Helicopter Individual-Blade-Control and Its Application to Gust Alleviation", Proc. Sixth European Rotorcraft Formum, Bristol, England, September 1980.

3. Ham, N.D. and Young, M.I., "Torsional Oscillation of Helicopter Blades Due to Stall", Journal of Aircraft, pp. 218-224, May-June 1966.

4. Quackenbush, T.R., "Testing and Evaluation of a Stall-Flutter-Suppression System for Helicopter Rotors Using Individual-Blade-Control", M.I.T. Aeroelastic and Structures Research Laboratory TR-196-3, August 1981.

$$\frac{\dot{\theta}_c}{I} = \frac{5000\,(1 + (s/195)^2)}{(1 + s/.366)(1 - s/p_1)(1 - s/\bar{p}_1)}$$

$$p_1 = -.057 + 200.1j$$

Using this and the feedback gains $K_\theta = .528$ and $K_{\dot{\theta}} = .19$, the closed loop transfer function for the servo block in Fig. 7 becomes

$$\frac{\theta_c}{V} = \frac{.131\,(1 + (s/195)^2)}{(1 + s/1230)(1 + s/161)(1 - s/p_2)(1 - s/\bar{p}_2)}$$

$$p_2 = -2.75 + 192.9j$$

TABLE 1

DESCRIPTION OF THE ROTOR BLADE USED IN WIND TUNNEL TESTS

No. of blades	1
Radius	2.311 ft.
Chord	2.0 in.
Section	NACA 0012
Rotational Speeds, Forward Flight Cases	6.7 Hz and 6.1 Hz
Elastic Axis	25% chord
Pitch Control Axis	25% chord
Hinge Offset (pitch/flap/lag)	2.0 in
Built-in Angle of Twist	8 deg. (linear)

APPENDIX

Development of System Dynamic Equations

Including the effects of the mechanical torsional spring, the equations of motion of the blade/servo system are:

$$\dot{I}L_a + IR + K_E\dot{\theta}_c = V \qquad (1)$$

$$-K_T I + J_T\ddot{\theta}_c + D\dot{\theta}_c + \frac{K_{NR}}{2}\left(\frac{\theta_c}{2} - \theta\right) = 0 \qquad (2)$$

$$J_B\ddot{\theta} + K_{NR}\,(\theta - \theta_c/2) = 0 \qquad (3)$$

where
- I = current through motor, amps
- V = voltage input to motor
- θ_c = angle of motor shaft, radius
- L_a = motor inductance
- R = motor resistance
- K_T = torque sensitivity
- K_E = volts back EMF
- D = motor viscous friction constant
- K_{NR} = non-rotating torsional spring constant of mechanical spring
- J_B = inertia of blade, clamps, and counterweights
- J_T = inertia of motor, tachometer, and linkage

Note the effects of the 2:1 reduction gear between the servomotor shaft and the blade in Eqs. (2) and (3). Equations 1, 2, and 3 yield the open loop transfer function (See left)

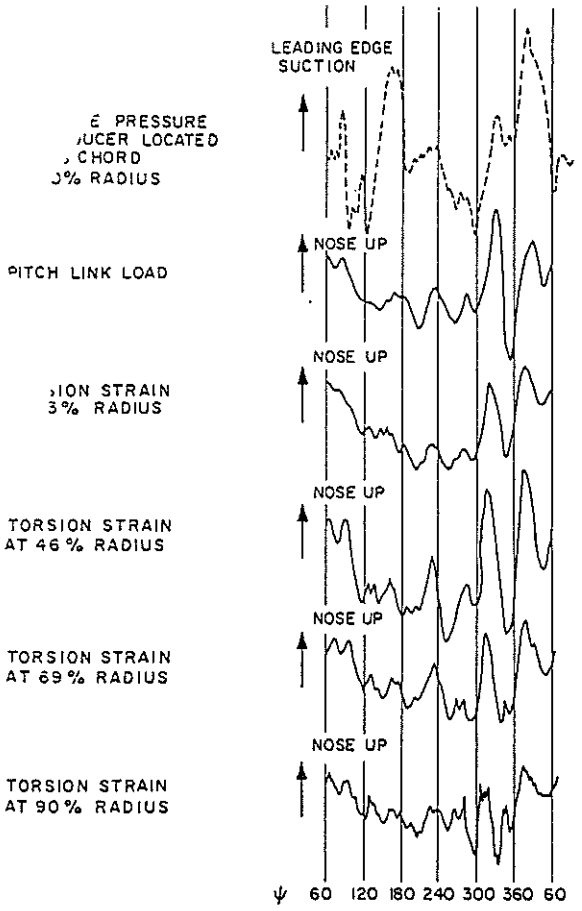

FIG. 1 Typical Torsion Loads on Blade Undergoing Stall Flutter

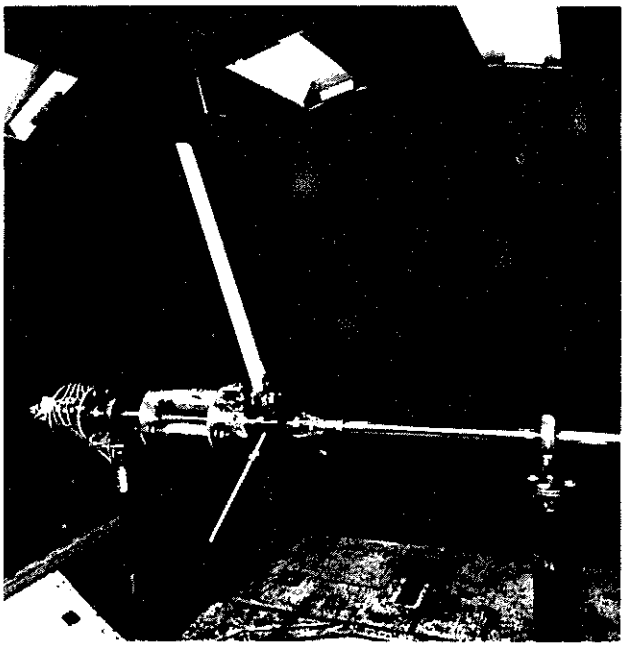

FIG. 3 Individual-Blade-Control Experimental Rig, Upstream View

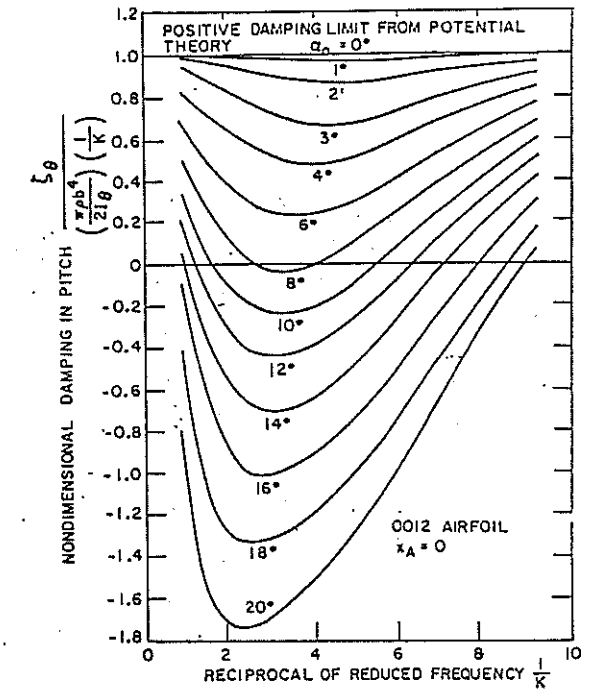

FIG. 2 Approximation for Generalized Pitch Damping

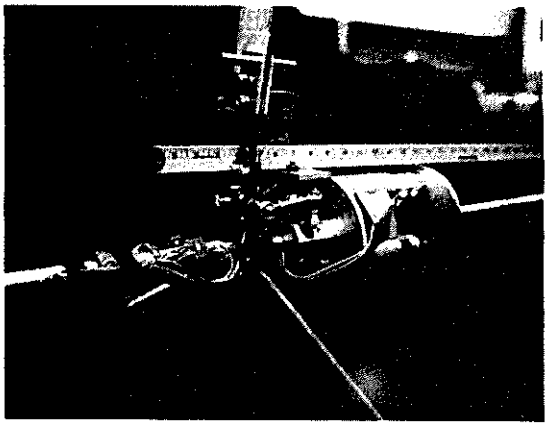

FIG. 4 View of Pitch Actuator and Blade Assembly

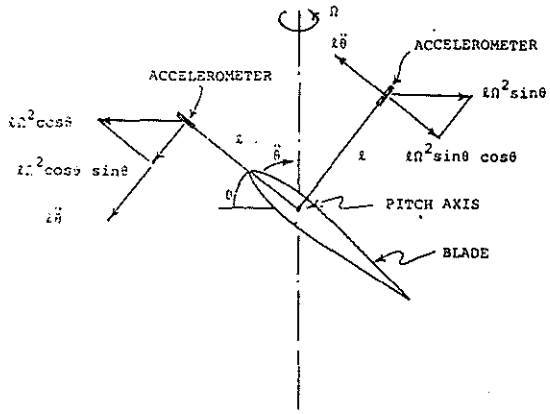

FIG. 5 Accelerometer Configuration

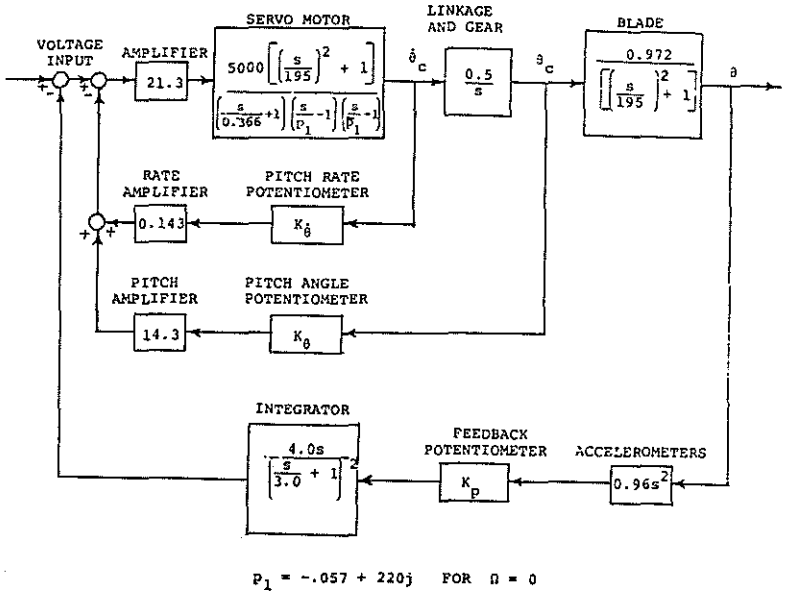

FIG. 6 Control System Block Diagram

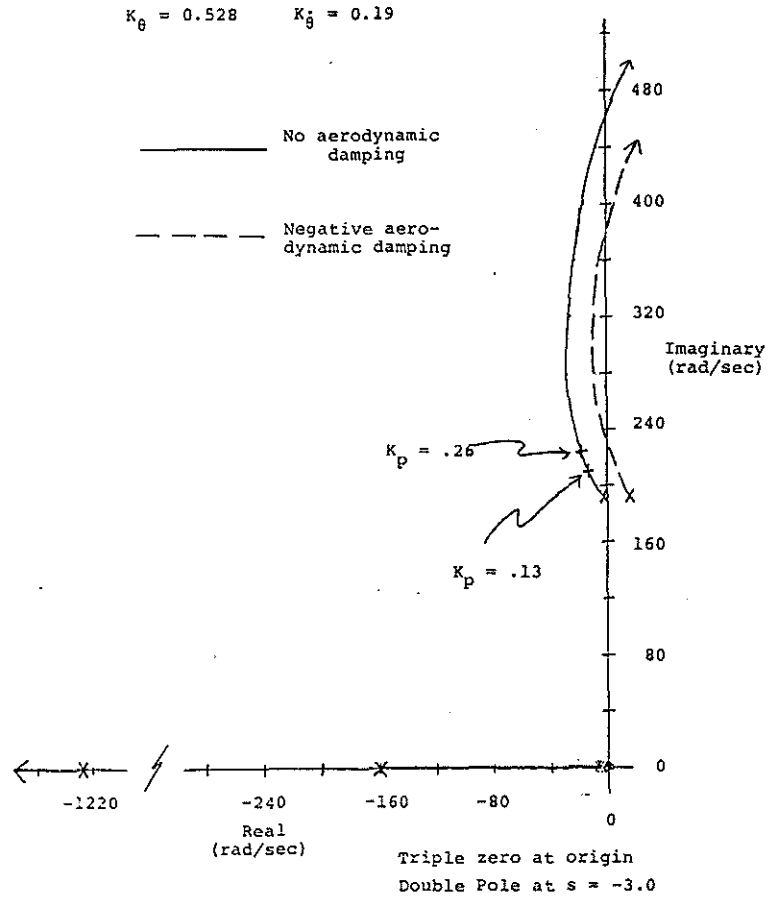

FIG. 7 Rcot Locus Diagrams, Static Tests with Mechanical Spring

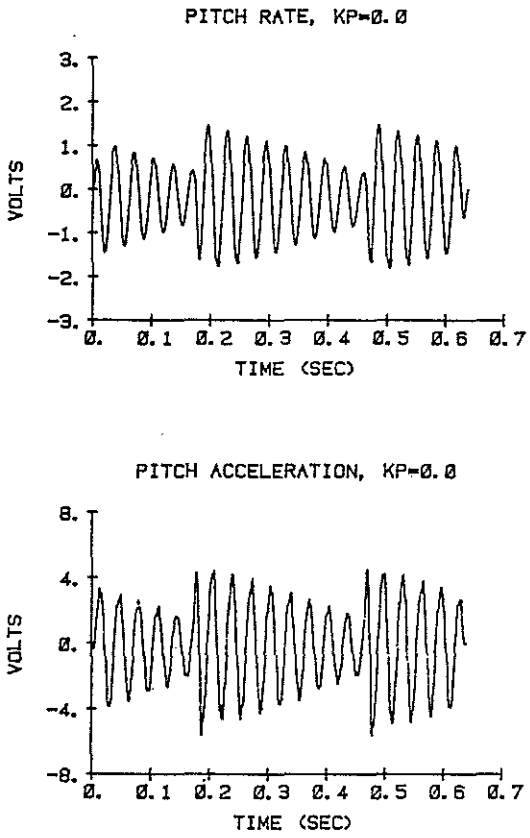

FIG. 8 Open-Loop, Static Mechanical Spring Tests

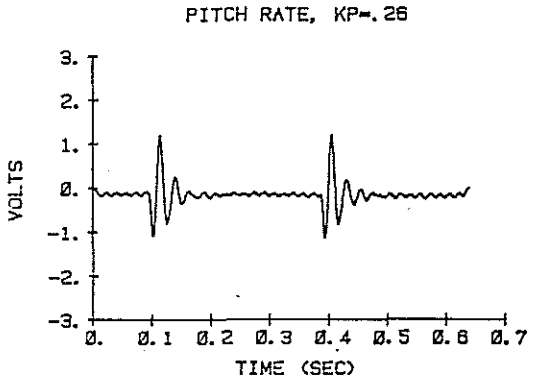

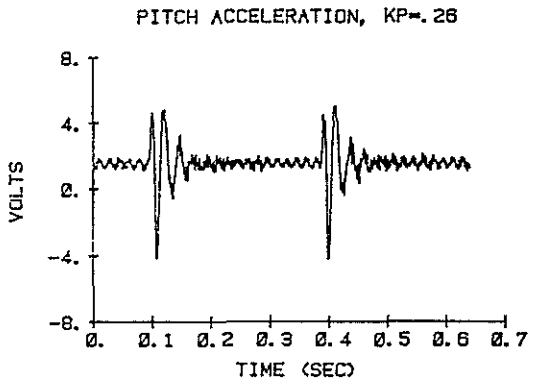

IG. 9 Static Mechanical Spring Tests, High Feedback

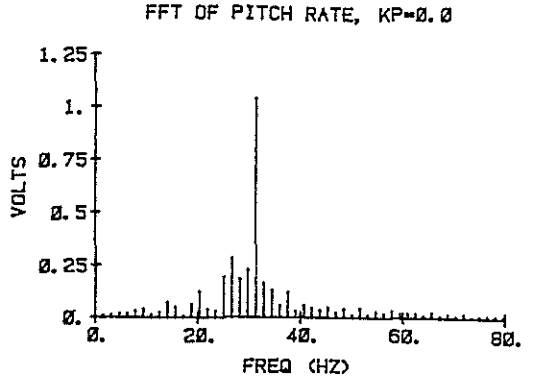

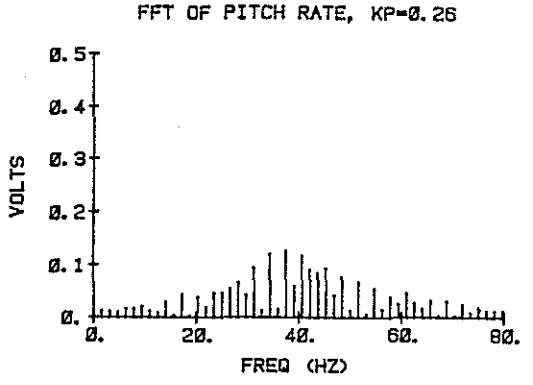

FIG. 10 Fourier Transforms of Static Mechanical Spring Responses

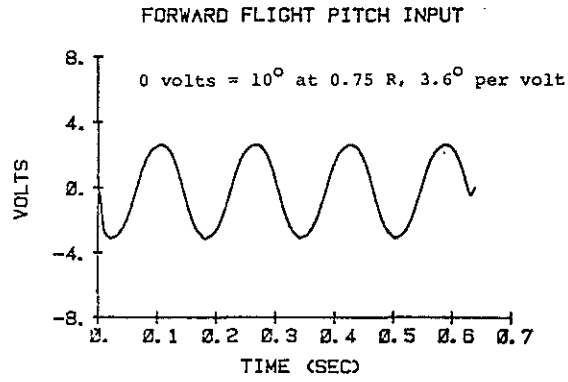

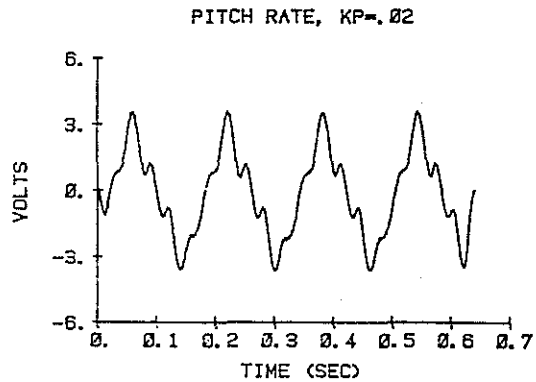

IG. 11 Low Feedback, Mechanical Spring Test, Ω = 6.1 Hz, μ = 0.33

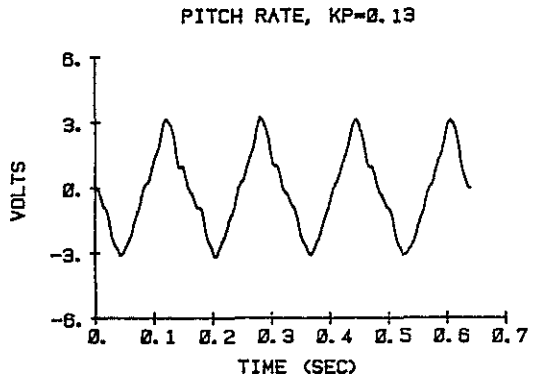

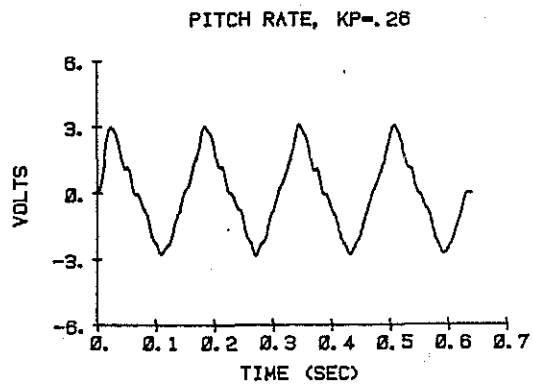

FIG. 12 Moderate and High Feedbacks, Mechanical Spring Test, Ω = 6.1 Hz, μ = 0.33

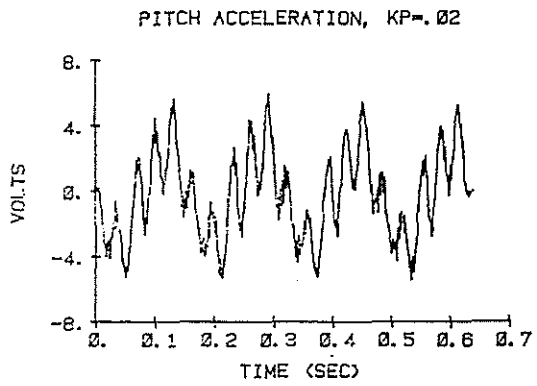

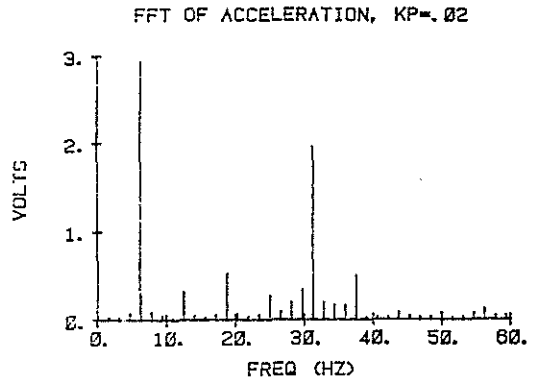

FIG. 13 Low Feedback Mechanical Spring Test, Ω = 6.1 Hz, μ = 0.33

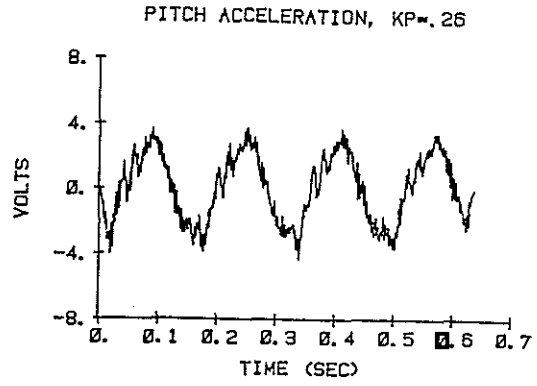

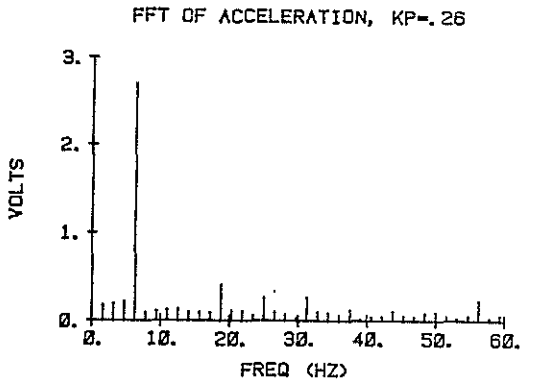

FIG. 14 High Feedback Mechanical Spring Test, Ω = 6.1 Hz, μ = 0.33

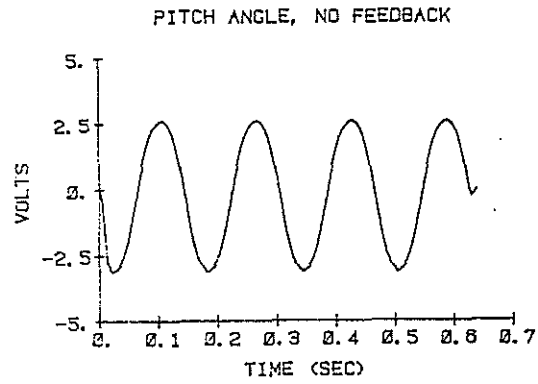

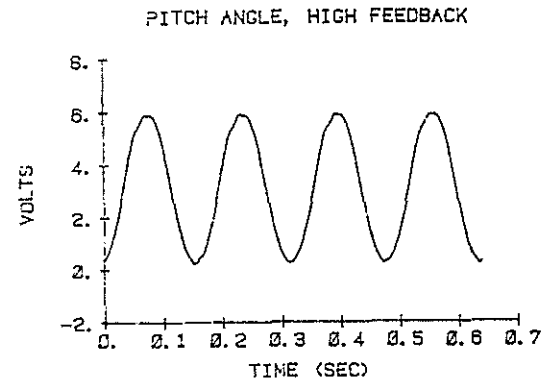

FIG. 15 Blade Pitch Input, Ω = 6.1 Hz, μ = 0.33

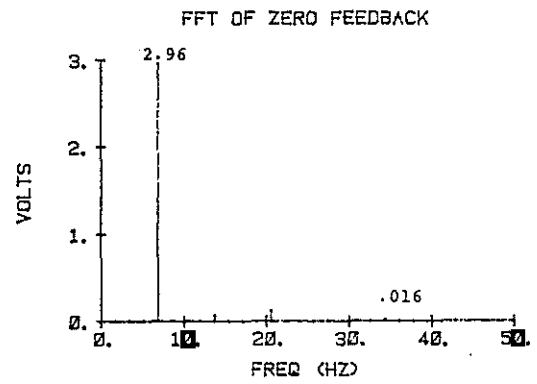

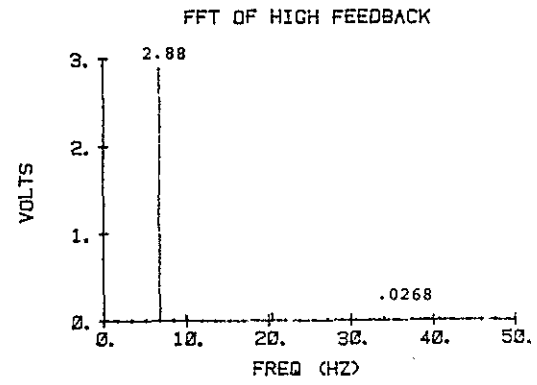

FIG. 16 Fourier Transforms of Pitch Input, Ω = 6.1 Hz, μ = 0.33